Energy and angular distribution of upward ultrahigh-energy neutrinos and signals of low scale gravity: Role of tau decay

Shahid Hussain* and Douglas W. McKay†
Department of Physics & Astronomy, University of Kansas, Lawrence, Kansas 66045, USA
(Received 12 October 2003; revised manuscript received 23 December 2003; published 6 April 2004)

We present extensive results and analysis of energy and angular distributions of diffuse UHE ν_e, ν_μ, and ν_τ fluxes propagated through Earth, with and without augmentation of the standard model interactions by low scale gravity. With propagated fluxes in hand we estimate event rates in a 1 km^3 detector in ice with characteristics of ICECUBE. We determine that, at an 0.5 PeV energy threshold, there is a significant difference in the ratios of down shower events to upward muon events between the standard model and the low scale gravity cases with 1 TeV and 2 TeV mass scales. The same is true for the energy threshold at 5 PeV. Though the difference is large in all flux models, the statistical significance of this difference depends on the flux models, especially at 5 PeV and above. Both flavor assumptions, ν_e, ν_μ, ν_τ::1, 2, 0 and ν_e, ν_μ, ν_τ::1, 1, 1, and all flux models show large differences. Though rates of tagged events are low, we find that ν_τ regeneration by τ decay may play an important role in disclosing deviations from standard model predictions at energies in the neighborhood of 1 PeV for 1-TeV-scale gravity, for example. We emphasize those analyses whose sensitivity to new physics is independent of the flux model assumed.

DOI: 10.1103/PhysRevD.69.085004 PACS number(s): 96.40.Tv, 04.50.+h, 13.35.Dx, 14.60.Pq

I. INTRODUCTION

The pursuit of high and ultrahigh energy neutrinos has greatly intensified over the past decade as more and more neutrino telescopes have entered the search. Though the observation of MeV neutrinos emitted from SN 1987a is over 15 years old [1,2], there is still no firm candidate for TeV, PeV or EeV neutrinos of galactic or extragalactic origin. Yet there is good reason to expect a neutrino flux exists in this energy regime because of the great success of air-shower detectors in building a detailed record of cosmic rays with these very-high to ultrahigh energies [3]. The photons or nuclear particles that are generally believed to initiate the observed shower are accompanied by neutrinos with similar energies, in most models of the high-energy particle emission by the sources. In any case, the neutrinos emitted by production and decay of pions by the highest energy primary cosmic rays as they interact with the cosmic microwave background, the so-called Greisen-Zatsepin-Kuzmin (GZK) [4] neutrinos, should be present at some level at ultrahigh energies [5], regardless of the mechanism responsible for producing the observed cosmic rays [6–8]. Even if there are no super-GZK neutrinos, there are a number of models [9–16] which predict the existence of neutrinos in the PeV–EeV range. By choosing several contrasting flux models and using enhanced cross sections from low scale gravity [17–19], we look for new physics effects that are relatively independent of flux models.

The expanding experimental capabilities and the strong theoretical interest in understanding the physics of astrophysical sources and particle interactions of the highest energy cosmic rays makes it imperative to study all aspects of the neutrino observation process. The number of groups reporting limits on fluxes and projecting improved limits with expanded data sets or with new facilities is impressive. In the range 1 TeV to 1 PeV, the AMANDA [20], Frejus [21], MACRO [22] and Baikal [23] experiments have reported limits on neutrinos from astrophysical (nonatmospheric) sources. In the range 1 PeV to 1 EeV, AGASA [24], AMANDA [25], Fly's Eye [26], and RICE [27] have all reported limits. Above 1 EeV, AGASA, Fly's Eye, GLUE [28] and RICE all put limits on the flux that extend up into the GZK range. The upper limits are getting interestingly close to the predictions of several models and actually below the predictions in several cases. The situation is heating up and will get hotter as the experiments like AUGER, which is already reporting preliminary results on air showers [29] and ICECUBE [30] are fully operational. Meanwhile, expanded data sets and improvements in sensitivity in experiments such as RICE will continue to search and to push down on limits until the first UHE neutrinos are observed [31].

These detection capabilities that have been achieved and will be improved and expanded in the next few years have direct impact on particle physics. The detection estimates, upon which limits are based, all rely on the extrapolation of neutrino cross sections well beyond the currently measured energy range. Is QCD correctly predicting these cross sections [32]? Is there new physics that enhances neutrino cross sections at high energies [33]? What is the effect of new neutrino interactions [34–40] or neutrino mixing [40–42] on the expected rates of detection in various telescopes? Clearly there is ample motivation for examining the consequences of various combinations of assumptions about the physics governing the cross sections and the assumptions about the flavor composition of the astrophysical flux of neutrinos. What, if any, are the observable distinctions among the various possibilities of flux and interaction characteristics? These questions and the experimental prospects for answers motivate this work.

*Electronic address: vacuum@ku.edu
†Electronic address: mckay@kuark.phsx.ku.edu

There is considerable published work on τ-neutrino propagation through Earth in *standard model (SM)* using analytic and computational tools [43–51] in the scenarios ν_e, ν_μ, ν_τ::1, 2, 0 and ν_e, ν_μ, ν_τ::1, 1, 1, and some analytical and computational work on neutrino propagation in low scale gravity (LSG) models has also been done in the ν_e, ν_μ, ν_τ::1, 2, 0 scenario [34,52]. A detailed study has not been done in the ν_e, ν_μ, ν_τ::1, 1, 1 scenario in LSG models. In this paper we solve, using Runge-Kutta method [53], the coupled differential equations for the four leptons ν_e, ν_μ, ν_τ, and τ in both of the above scenarios, in SM and LSG models. For cross section calculations, we use Gaussian and Monte Carlo integration methods [53] with CTEQ6-DIS parton distributions [54]. Our results confirm significant regeneration effect due to taus in the SM as already shown by several authors [46,47]. However, as we will see the regeneration due to taus is not as significant in LSG models. Also, by comparing results of [46,47], one finds that electromagnetic (EM) losses of τ are not making a significant difference in the SM fluxes of ν_τ around 1 PeV, hence, we do not include EM losses in our work here. As we will see in the next section, EM losses are not important at all in LSG models.

In Sec. II we talk about cross sections and interaction lengths in SM and LSG; Sec. III gives the formalism for neutrino propagation through the Earth; in Sec. IV we show our results for different neutrino models and discuss them; in Sec. V we develop formalism for event rates calculation and in Sec. VI we show and discuss our results for event rates; Sec. VII gives the summary of our results and the conclusion.

II. CROSS SECTIONS AND INTERACTION LENGTHS

Before evaluating the equations of propagation for the four leptons ν_e, ν_μ, ν_τ, and τ through the Earth in the next section, we need to calculate their cross sections on isoscalar nucleons [$N=(p+n)/2$], where n stands for neutron and p for proton. We need to calculate their neutral current (NC) and charged current (CC) weak interaction cross sections in SM and eikonal (EK) and black hole (BH) cross sections in LSG models. The LSG models do not discriminate among different particles; they are the same for all the four leptons ν_e, ν_μ, ν_τ, and τ. The SM total cross sections for different flavors are also the same within a few percent at the ultrahigh energies we are interested in here. We will assume the SM cross sections are the same for all the four leptons ν_e, ν_μ, ν_τ, and τ, and we will use ν_μ NC and CC cross sections for all of them. The differences between τ and ν weak cross sections are not important because τ decay is the only dominant process for τ's up to energies 10^8 GeV, and at higher energies the differences are not significant anyway [55]. A detailed discussion of SM ν_μ-nucleon cross sections is given in Ref. [56]. We have used CTEQ6-DIS parton distributions. Details of calculation for LSG model cross sections are given in Refs. [34,57], where CTEQ4-DIS parton distributions [58] were used. The difference between CTEQ4-DIS and CTEQ6-DIS cross section calculations is not significant. We outline the LSG calculation here so that the presentation is reasonably self-contained.

The classical gravity Schwarzschild radius $r_S(\sqrt{s})$ is the dominant physical scale when the collision energy is large compared to the Plank mass. At impact parameters smaller than r_S, we use the parton-level geometrical cross section [59]

$$\hat{\sigma}_{\rm BH} \approx \pi r_S^2. \tag{1}$$

For values of the classical impact parameter, b, larger than r_s we use the contributions to the amplitude in the eikonal approximation. In Eq. (1), r_S is the Schwarzchild radius of a $(4+n)$-dimensional black hole of mass $M_{\rm BH}=\sqrt{\hat{s}}$ [60],

$$r_S = \frac{1}{M}\left[\frac{M_{\rm BH}}{M}\right]^{1/(1+n)}\left[\frac{2^n \pi^{(n-3)/2}\Gamma\left(\frac{3+n}{2}\right)}{2+n}\right]^{1/(1+n)}, \tag{2}$$

where $\sqrt{\hat{s}}$ is the neutrino-parton c.m. energy, and M is the $(4+n)$-dimensional scale of quantum gravity. Multiplying by the parton distribution functions, $f_i(x,q)$, choosing q at a value characteristic of black hole production and integrating over momentum fraction x, gives the estimate

$$\sigma_{\nu N\to BH}(s) = \sum_i \int_{x_{min}}^1 dx \hat{\sigma}_{BH}(xs) f_i(x,q). \tag{3}$$

We take $x_{min}=M^2/s$ and $q=\sqrt{\hat{s}}$. The dependence of $\sigma_{\nu N\to BH}(s)$ on the choice of x_{min} and the treatment of q is discussed in Refs. [61–64].

For the input amplitude to the eikonal approximation, referred to as the Born amplitude, we choose

$$i\mathcal{M}_{\rm Born} = \sum_j \frac{ics^2}{M^2}\frac{1}{q^2+m_j^2}, \tag{4}$$

where c is the gravitational coupling strength, $c=(M/\bar{M}_P)^2$ and $\bar{M}_P=2.4\times10^{18}$ GeV is the reduced, four dimensional Planck mass. Here $q=\sqrt{-t}$ is the usual lepton momentum transfer. The index j must include the mass degeneracy for the jth KK mode mass value. The sum, which can be well approximated by an integral, must be cut off at some scale, generally taken to be of the order of M. The transverse Fourier transform of the Born amplitude produces the eikonal phase as a function of impact parameter b,

$$\chi(s,b) = \frac{i}{2s}\int \frac{d^2q}{4\pi^2}\exp(i\mathbf{q}\cdot\mathbf{b}) i\mathcal{M}_{\rm Born}. \tag{5}$$

Evaluating the integral over q and representing the sum in the Born term by an integral, one finds the ultraviolet-finite result

$$\chi(s,b) = -\frac{s(2^{2n-3}\pi^{3n/2-1})}{M^{n+2}\Gamma(n/2)} 2\int_0^\infty dm m^{n-1} K_0(mb)$$

$$= \left(\frac{b_c}{b}\right)^n, \tag{6}$$

where

$$b_c^n = \frac{1}{2}(4\pi)^{n/2-1}\Gamma\left[\frac{n}{2}\right]\frac{s}{M^{2+n}}. \tag{7}$$

The eikonal amplitude is then given in terms of the eikonal phase by

$$\mathcal{M} = -2is\int d^2b\,\exp(i\mathbf{q}\cdot\mathbf{b})[\exp(i\chi)-1]$$

$$= -i4\pi s\int dbbJ_0(qb)[\exp(i\chi)-1]. \tag{8}$$

The eikonal amplitude can be obtained analytically [65–67] in the strong coupling $qb_c \gg 1$ and weak coupling $qb_c \ll 1$ limits.

For strong coupling, the stationary phase approximation is valid, yielding

$$\mathcal{M} = A_n e^{i\phi_n}\left[\frac{s}{qM}\right]^{(n+2)/(n+1)}, \tag{9}$$

where

$$A_n = \frac{(4\pi)^{3n/(2(n+1))}}{\sqrt{n+1}}\left[\Gamma\left(\frac{n}{2}+1\right)\right]^{1/(1+n)}, \tag{10}$$

$$\phi_n = \frac{\pi}{2} + (n+1)\left[\frac{b_c}{b_s}\right]^n, \tag{11}$$

and $b_s = b_c(qb_c/n)^{-1/(n+1)}$. In the cross section calculation, we set the amplitude equal to its value at $q = 1/b_c$ for values of q that are less than $1/b_c$, since the small q region makes negligible contribution to the cross section.

We assume that the black hole cross section is the dominant one for $q \geqslant 1/r_S$. The eikonal cross section is cut off at this value of q, since it is not expected to be reliable for values of q larger than $1/r_S$ in any case.

In Fig. 1 we plot the SM and LSG (models with mass scale 1 TeV and 2 TeV; $n=6$) neutrino-isoscalar nucleon cross sections. For SM we plot neutral current (NC), charged current (CC), and total (NC+CC) cross sections. For LSG we plot eikonal (EK), black hole (BH), and total (EK + BH) cross sections. We see σ_{BH} is larger then σ_{EK} for our case ($n=6$). However, in $n=3$ case not shown here, the reverse is true. Our results turned out to be only marginally sensitive to the number of dimensions, so we choose to work with $n=6$, for which the bound on the scale M is the weakest.

The interaction length in a material with density ρ is defined here as $\mathcal{L}_{int} = (1/N_A\rho\sigma)$, where N_A is Avogadro's number and σ is the cross section for the interaction. Figure 2 gives the interaction lengths in SM and LSG as well the τ-decay length. We set $\rho = 8.0\ \mathrm{g\,cm^{-3}}$ to make some comparisons between the interaction lengths and the electromagnetic (em) ranges of taus and muons given in Ref. [45], using this value of ρ.

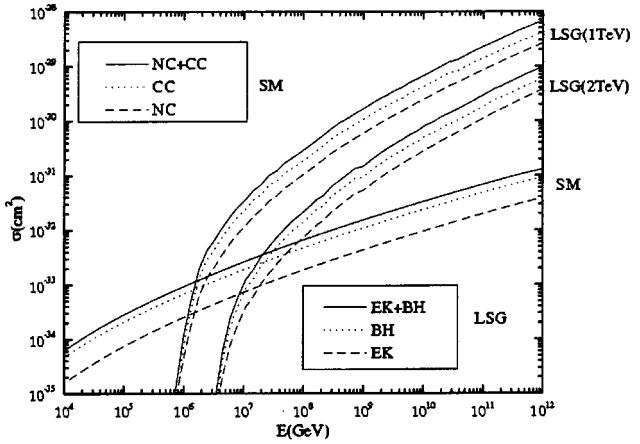

FIG. 1. ν_μ–isoscalar nucleon cross sections (cm^2) vs energy (GeV): for low scale gravity (LSG) models, with number of extra dimensions $n=6$, we plot eikonal (EK, dashed line), black hole (BH, dotted line), and total (EK+BH, solid line) cross sections; for standard model (SM) we plot neutral current (NC, dashed line), charged current (CC, dotted line), and total (NC+CC, solid line) cross sections.

Which particles do we need to include in our propagation of neutrinos through the Earth? We have six candidates which might be coupled with each other: ν_e, ν_μ, ν_τ, and their three leptonic partners. One can exclude electrons from this list, both in SM and LSG, because they shower electromagnetically before they produce any ν_e through the CC interaction at energies of our interest here. The case for μ's and τ's needs some attention because it is different in SM

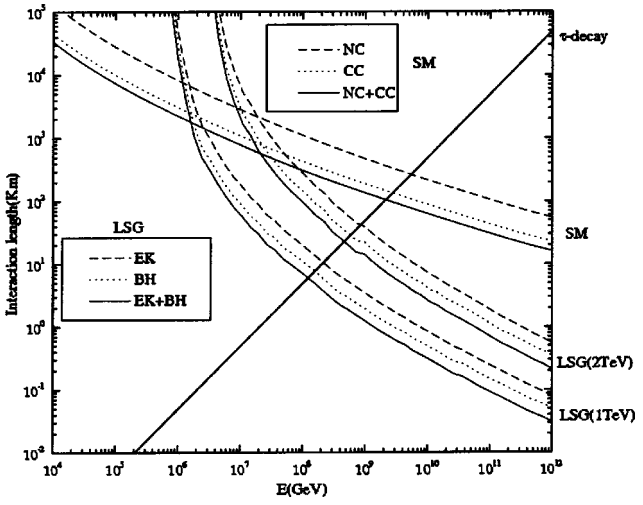

FIG. 2. Interaction lengths (km) vs energy (GeV): interaction length $\mathcal{L}_{int} = 1/\sigma(E)N_A\rho$, where $\sigma(E)$ are plotted in Fig. 1, N_A is Avogadro's number, and ρ is the material density; we choose $\rho = 8\ \mathrm{g\,cm^{-3}}$ to make some comparisons with Ref. [45]. For low scale gravity (LSG) models, with number of extra dimensions $n=6$, we plot eikonal (EK, dashed line), black hole (BH, dotted line), and total (EK+BH, solid line) interaction lengths. For standard model (SM) we plot neutral current (NC, dashed line), charged current (CC, dotted line), and total (NC+CC, solid line) interaction lengths. We also plot τ-decay length (thick solid line).

and LSG. In SM we can ignore μ's but not τ's because of the comparatively smaller decay length and larger EM ranges of taus. For LSG, muons play some role in the propagation through the Earth at high enough energy as explained below. The effect is quite small, however.

If we look at the interaction lengths and τ-decay length in Fig. 2, we find that (i) the LSG1 model (LSG model with mass scale 1 TeV) interaction lengths become smaller than the τ-decay length for $E>10^8$ GeV. This implies the regeneration effect due to taus will be suppressed in LSG models (ii) if we look at the EM ranges of taus [45], we find that the LSG1 model interaction lengths become smaller than the tau EM range for $E>10^8$ GeV. This gives a reason for not including, in LSG, the EM energy losses of taus in our propagation of neutrinos, coupled with taus, through the Earth. (iii) If we look at the EM ranges of muons [45], we find that even the muon EM energy losses are not important for $E>10^8$ GeV. (iv) Given the above reasons, interestingly, taus and muons become almost identical in LSG for $E>10^8$ GeV. This means one may have to treat muons and taus on equal footing in the propagation of neutrinos through the Earth for $E>10^8$ GeV in LSG1 model and for $E>10^9$ GeV in LSG2 model (LSG model with mass scale 2 TeV). However, in the present work, we do not include muons in the propagation equations because we are looking at neutrinos around 1 PeV here, and we expect the coupling of muons with the ν_μ via CC interaction for $E>10^8$ GeV will not affect the neutrino flux much around 1 PeV by feed down; the muon decay length, being so large in contrast to that of τ, will play no role in regeneration of ν_μ [45].

III. NEUTRINO PROPAGATION THROUGH EARTH

Here we discuss the coupled propagation of ν_e, ν_μ, ν_τ, and τ through Earth. We do not include the EM energy losses of taus for the reasons discussed in the previous section. Suppose we have a differential flux [83] $F^i(E,x,\theta)$ of lepton of species i at the surface of Earth, then the transport equation for each of the four leptons is

$$\frac{dF^i(E,x,\theta)}{dx} = -N_A\rho(x,\theta)F^i(E,x,\theta)\sigma_t^i(E) - \frac{F^i(E,x,\theta)}{\mathcal{L}^i_{dec}(E)} + \sum_j \left[N_A\rho(x,\theta)\int_E^\infty dE' F^j(E',x,\theta) \times \frac{d\sigma^{j\to i}(E',E)}{dE} + \int_E^\infty dE' F^j(E',x,\theta)\frac{dP^{dec(j\to i)}(E',E)}{dE}\right], \tag{12}$$

where the first two terms give the loss and the last two terms give gain of the flux per unit length in the same energy bin E. Avogadro's number N_A times the density $\rho(x,\theta)$, gives the number of target nucleons per unit volume at the nadir angle θ and distance x in the Earth (see Fig. 3). We use the Earth density model from Ref. [68]. $\sigma_t^i(E)$ is the total cross section for a lepton of flavor i to interact with a nucleon and be expelled from the energy bin E:

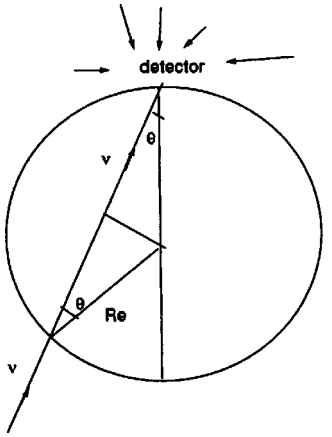

FIG. 3. Drawing of the Earth: θ is the nadir angle and Re is the radius of the Earth. Arrows outside the Earth represent the down flux. Upflux is the flux coming through the Earth.

$$\sigma_t^i(E) = \sigma^i_{CC}(E) + \sigma^i_{NC}(E) + \sigma^i_{BH}(E) + \sigma^i_{EK}(E),$$

where we use the same $\sigma_t^i(E)$ for all the four leptons ν_e, ν_μ, ν_τ, and τ (LSG cross sections are the same for them; see Sec. II for discussion on SM cross sections). The second term in Eq. (12) gives the loss due to decays. It is zero for the neutrinos, and for taus

$$\mathcal{L}^\tau_{dec}(E) = \gamma c \mathcal{T}, \tag{13}$$

where $\gamma = E_\tau/m_\tau$ is the Lorentz factor, $\mathcal{T}$ is the mean life time of taus, and c is the speed of light in vacuum. The third term in Eq. (12) gives the gain in the flux of species i in the bin E, resulting from interaction of the species j at $E'>E$, and

$$\sum_j \frac{d\sigma^{j\to i}(E',E)}{dE} = \frac{d\sigma^{i\to i}_{NC}(E',E)}{dE} + \frac{d\sigma^{j\to i(i\neq j)}_{CC}(E',E)}{dE} + \frac{d\sigma^{i\to i}_{EK}(E',E)}{dE}.$$

In the above equation, there is no need for the second term on the right-hand side for ν_e and ν_μ propagation equations as we are not keeping track of electrons and muons for the reasons given in the last section. However, we keep this term for the ν_τ and τ equations as we are propagating taus along with the neutrinos. For the reasons given earlier, we use the same NC, CC, EK differential cross sections for all the four leptons in the above equation. The fourth term in Eq. (12) is the gain in flux of species i in the bin E due to tau decays. This term is zero in the tau flux equation. For ν_e, ν_μ, and ν_τ we consider the corresponding decay channels of taus as formulated in [46], [2000]: (i) $\tau\to\nu_\tau\mu\nu_\mu$, (ii) $\tau\to\nu_\tau e\nu_e$, (iii) $\tau\to\nu_\tau\pi$, (iv) $\tau\to\nu_\tau\rho$, (v) $\tau\to\nu_\tau a1$, and (vi) $\tau\to\nu_\tau X$. These decays have branching ratios of 0.18, 0.18, 0.12, 0.26, 0.13,

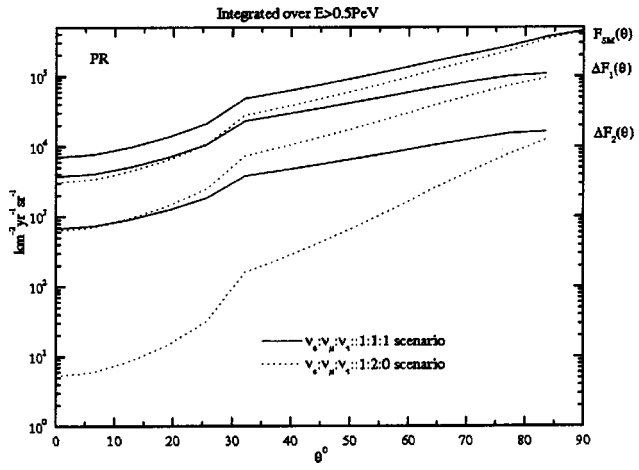

FIG. 4. Upward neutrino flux (km^{-2}yr^{-1}sr^{-1}) integrated over energy $E>0.5$ PeV vs nadir angle θ (deg) for Protheroe input flux model: SM upward neutrino flux $F_{SM}(\theta)$, and flux differences $\Delta F_1(\theta)$ and $\Delta F_2(\theta)$, as defined in Eqs. (14) and (15), are plotted for two scenarios: $\nu_e:\nu_\mu:\nu_\tau$::1:1:1 (solid lines) and $\nu_e:\nu_\mu:\nu_\tau$::1:2:0 (dotted lines).

0.13 [69], respectively. All the decays give a ν_τ. The first two decays couple the tau propagation with ν_e and ν_μ propagation. The last decay includes the rest of the hadronic decays not specified in (iii) through (vi). For a review, see [70,71].

IV. RESULTS AND DISCUSSION FOR FLUXES

Below we show results for total fluxes, including all the neutrino species and their respective antineutrinos, unless defined otherwise. We plot upward fluxes instead of up-to-down flux ratios to find the region in the (E,θ) space to compare the SM and LSG models in terms of absolute flux

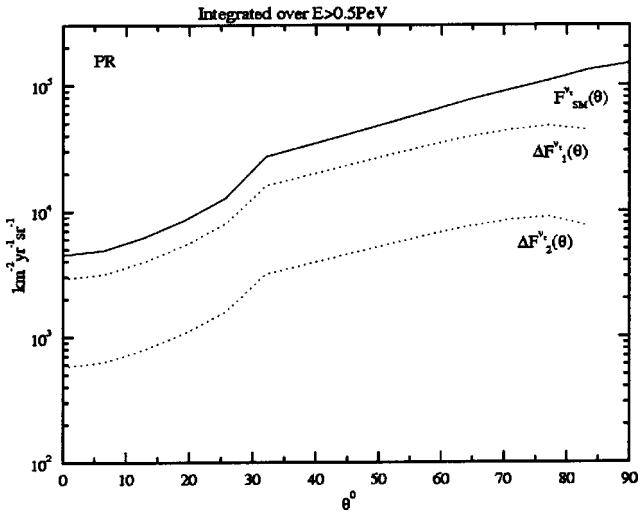

FIG. 5. Upward ν_τ flux (km^{-2}yr^{-1}sr^{-1}) integrated over energy $E>0.5$ PeV vs nadir angle θ (deg) for Protheroe input flux model: SM upward ν_τ flux $F^{\nu_\tau}_{SM}(\theta)$ (solid line), and ν_τ flux differences $\Delta F^{\nu_\tau}_1(\theta)$ and $\Delta F^{\nu_\tau}_2(\theta)$ (dotted lines), as defined in Eqs. (14) and (15), for the scenarios: $\nu_e:\nu_\mu:\nu_\tau$::1:1:1.

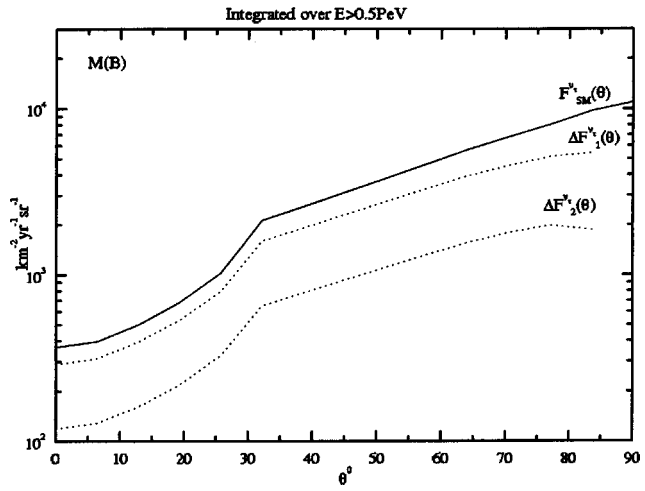

FIG. 6. Same as Fig. 5, but with Mannheim (B) flux model.

differences. Larger fluxes mean more events, and larger difference in the number of neutrinos in SM and LSG means better chances to differentiate between the models. The ratio plots are not always helpful for that purpose because they do not show us the actual number of neutrinos and the flux difference of the SM and LSG. We present plots for $\Delta F_1(E,\theta)$, $\Delta F_2(E,\theta)$ in the (E,θ) space, where

$$\Delta F_1(E,\theta)=F_{SM}(E,\theta)-F_{LSG1}(E,\theta) \tag{14}$$

and

$$\Delta F_2(E,\theta)=F_{SM}(E,\theta)-F_{LSG2}(E,\theta). \tag{15}$$

Here $F_{LSG1}(E,\theta)$, $F_{LSG2}(E,\theta)$ are the total upward fluxes in the low scale gravity models with mass scale 1 TeV and 2 TeV, respectively, and number of extra dimensions $n=6$. $F_{SM}(E,\theta)$ is the upward flux in standard model. $\Delta F_1(E)$, $\Delta F_2(E)$, $\Delta F_1(\theta)$, and $\Delta F_2(\theta)$ are defined in the same manner as $\Delta F_1(E,\theta)$ and $\Delta F_2(E,\theta)$ are defined above.

Below we show our analysis for the neutrino flux models due to Protheroe [11], Mannheim (B) [12], Waxman Bahcall [10], SDSS [9], and $1/E$ generic model. Though we did not show it here, we also looked at atmospheric and galactic neutrinos [72] around 0.5 PeV. However, the up fluxes in this case are ignorable as compared to the above extragalactic flux models: the galactic up flux is more than an order of magnitude smaller than the up flux from any of the flux models considered here; the atmospheric up flux is more than two orders of magnitude lower than even the galactic up flux. The reason is quite simple: one should expect larger feed down in the upward model fluxes considered here; these extragalactic models have much larger fluxes above 1 PeV than the atmospheric or galactic fluxes. As a result, the model fluxes at higher energies give larger feed down at 0.5 PeV while the atmospheric and galactic up fluxes are so small there that they give essentially no feed down. This is especially true in SM because of the strong feed down effect per incident ν_τ due to tau decays, which may make the extragalactic model up fluxes, in SM, large enough to be detectable even at 0° nadir angles around 0.5 PeV.

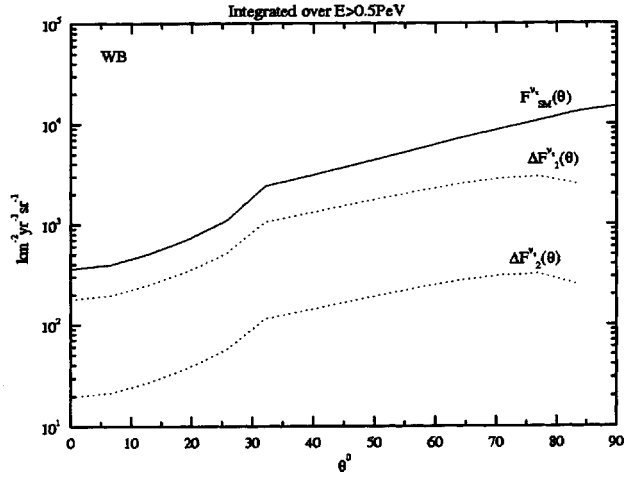

FIG. 7. Same as Fig. 5, but with Waxman Bahcall (WB) flux model.

We will first show some plots (Figs. 4–14) to explore (E,θ) space of the neutrino fluxes, and finally we will give two tables of numbers for different neutrino flavor flux ratios. Three types of plots are shown below:

(i) Fluxes integrated over energy vs nadir angle. Figures 4 and 5 refer to our example of Protheroe [11] model. Figure 4 shows the angular distribution of the total SM flux $F_{SM}(\theta)$ integrated over energy $E>0.5$ PeV, along with the flux differences $\Delta F_1(E)$ and $\Delta F_2(E)$ as defined in Eqs. (14) and (15). The qualitative features of Figs. 4 and 5 are the same in every flux model, so we do not show figures for the other flux models corresponding to Fig. 4. However, we show the corresponding figures for Fig. 5 for the four models [Protheroe [11], Mannheim (B) [12], Waxman Bahcall [10], SDSS [9]] because our emphasis here is on τ effects, and we wish to show their qualitative features are independent of the flux model. As mentioned earlier, the atmospheric and galactic [72] up fluxes are not significant as compared to the four extragalactic source models at these energies, so we do not consider them here.

We plot the upward fluxes in two scenarios for the initial flux: ν_e, ν_μ, ν_τ::1, 1, 1 (solid lines) and ν_e, ν_μ, ν_τ::1, 2, 0 (dotted lines). The two scenarios correspond to $\nu_\mu \rightarrow \nu_\tau$ oscillations and no oscillations in space, respectively. The following observations are common to all models and are relevant to Fig. 4: (i) the difference is largest in number around 75°–85°; however, as we will see in 3D plots in (E,θ) space, the maximum of the difference shifts to lower angles at lower energies; (ii) around 30° nadir angle, one can clearly see the effect of the core—stronger suppression; (iii) the difference in flux between SM and LSG models is larger at any angle in the ν_e, ν_μ, ν_τ::1, 1, 1 scenario than in the no tau scenario. This is expected because of the stronger tau regeneration effect in the SM as compared to LSG; in LSG, the black hole cross section, being the largest of all as shown

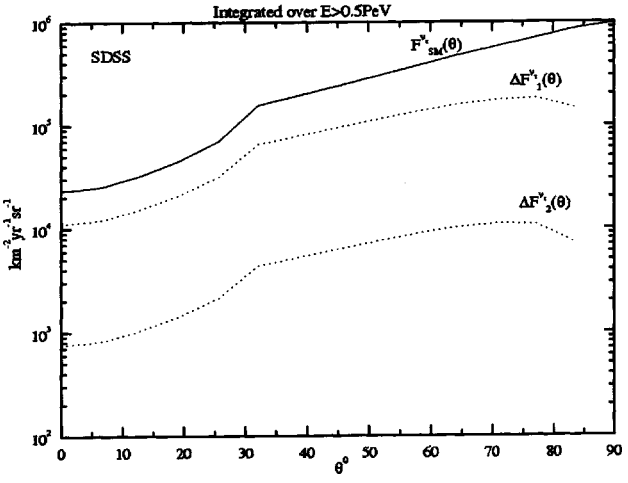

FIG. 8. Same as Fig. 5, but with SDSS flux model.

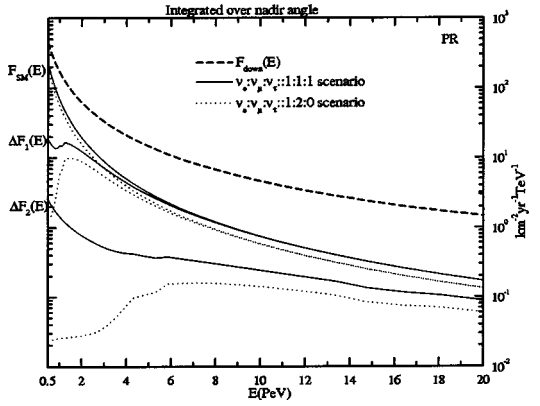

FIG. 9. Upward neutrino flux (km^{-2}yr^{-1}TeV^{-1}) integrated over nadir angle vs energy E (PeV) for Protheroe input flux model: SM upward neutrino flux $F_{SM}(E)$, and flux differences $\Delta F_1(E)$ and $\Delta F_2(E)$, as defined in Eqs. (14) and (15), are plotted for two scenarios: $\nu_e:\nu_\mu:\nu_\tau$::1:1:1 (solid lines), and $\nu_e:\nu_\mu:\nu_\tau$::1:2:0 (dotted lines). Also shown is the downward Protheroe model flux, integrated over nadir angle (dashed line).

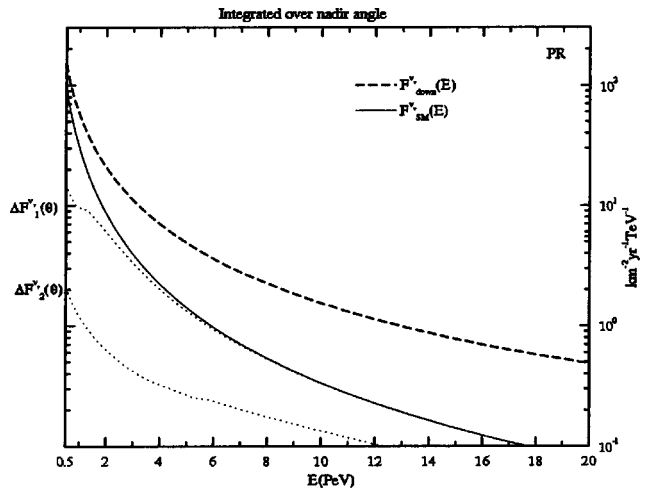

FIG. 10. Upward ν_τ flux (km^{-2}yr^{-1}TeV^{-1}) integrated over nadir angle vs energy E (PeV) for Protheroe input flux model: SM upward ν_τ flux $F^{\nu_\tau}_{SM}(E)$ (solid line), and ν_τ flux differences $\Delta F^{\nu_\tau}_1(E)$, and $\Delta F^{\nu_\tau}_2(E)$ (dotted lines), as defined in Eqs. (14) and (15), for the scenarios: $\nu_e:\nu_\mu:\nu_\tau$::1:1:1. Also shown is the downward ν_τ Protheroe model flux, integrated over nadir angle (dashed line).

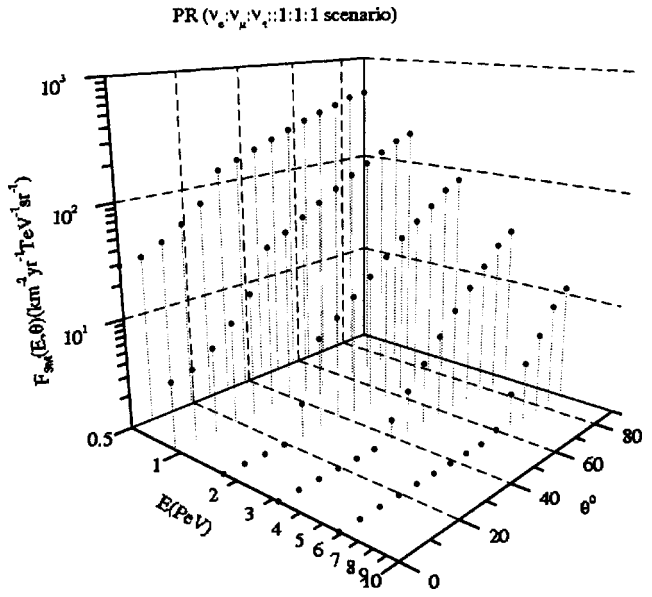

FIG. 11. SM upward neutrino flux $F_{SM}(E,\theta)$ ($\mathrm{km}^{-2}\mathrm{yr}^{-1}\mathrm{TeV}^{-1}\mathrm{sr}^{-1}$) vs energy E (PeV) and nadir angle θ (deg), for Protheroe input flux model in the scenario $\nu_e:\nu_\mu:\nu_\tau::1:1:1$.

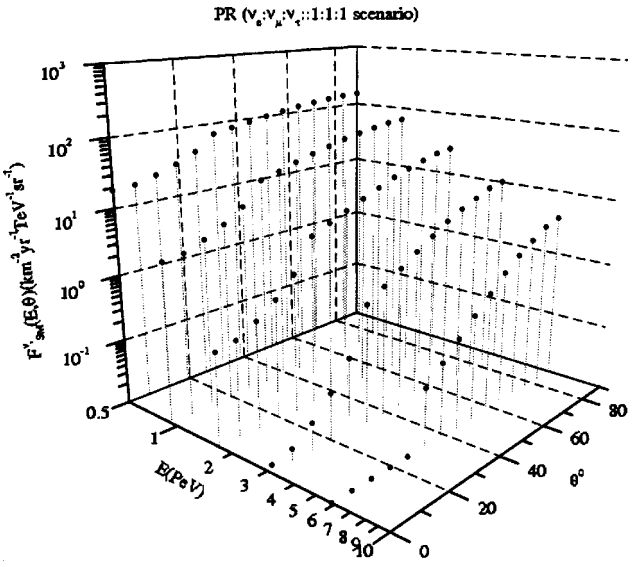

FIG. 13. SM upward ν_τ flux $F_{SM}(E,\theta)$ ($\mathrm{km}^{-2}\mathrm{yr}^{-1}\mathrm{TeV}^{-1}\mathrm{sr}^{-1}$) vs energy E (PeV) and nadir angle θ (deg), for Protheroe input flux model in the scenario $\nu_e:\nu_\mu:\nu_\tau::1:1:1$.

in Fig. 1, suppresses regeneration due to any process. This observation leads us to concentrate on tau fluxes only, as discussed below.

In Figs. 5–8 we show the same plots for ν_τ as was shown for the total fluxes. We plot these figures for all four models: Protheroe [11], Mannheim (B) [12], Waxman Bahcall [10], and SDSS [9]. In these figures, the solid line is the ν_τ flux in SM and the two dotted lines are the difference fluxes [see Eqs. (14), (15)] for ν_τ. We clearly see that in LSG1 model, regardless of the flux model, difference in ν_τ fluxes is more than 50% of the total difference due to all neutrino species. For example, the ν_τ difference $\Delta F_1(E)$ (Fig. 5) for Protheroe model at 0° nadir angle is around 3000, while the total difference is around 4000 (Fig. 4), $\mathrm{km}^{-2}\mathrm{yr}^{-1}\mathrm{sr}^{-1}$. This behavior is independent of the flux models—about 3/4 of the total difference is due to ν_τ only. This may be useful as ICECUBE is expected to differentiate between neutrino flavors around 500 TeV [73].

(ii) Flux integrated over nadir angle vs energy. The fluxes integrated over nadir angle do not show as much detail as the ones integrated over energy. This is because the integrated flux gets dominant contribution from nadir angles around 90° where the chord length of the Earth is not long enough to make the difference between SM and LSG prominent. For this reason, it suffices to show plots for only one flux model,

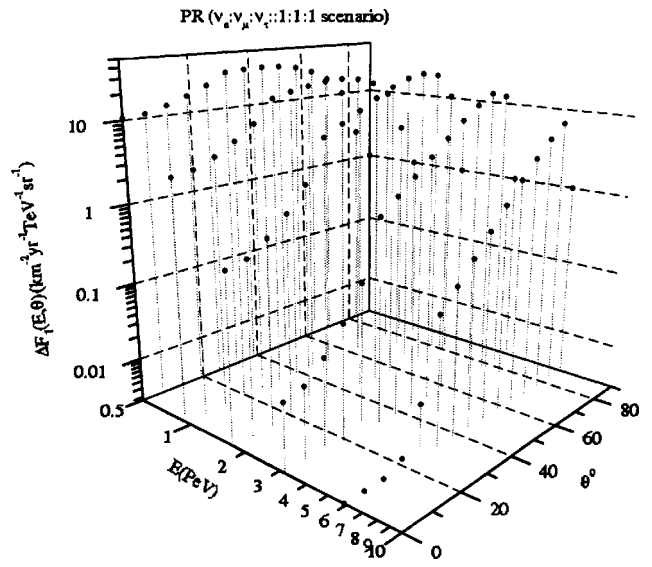

FIG. 12. Upward neutrino flux difference $\Delta F_1(E,\theta)$ ($\mathrm{km}^{-2}\mathrm{yr}^{-1}\mathrm{TeV}^{-1}\mathrm{sr}^{-1}$) vs energy E (PeV) and nadir angle θ (deg), for Protheroe input flux model in the scenario $\nu_e:\nu_\mu:\nu_\tau::1:1:1$.

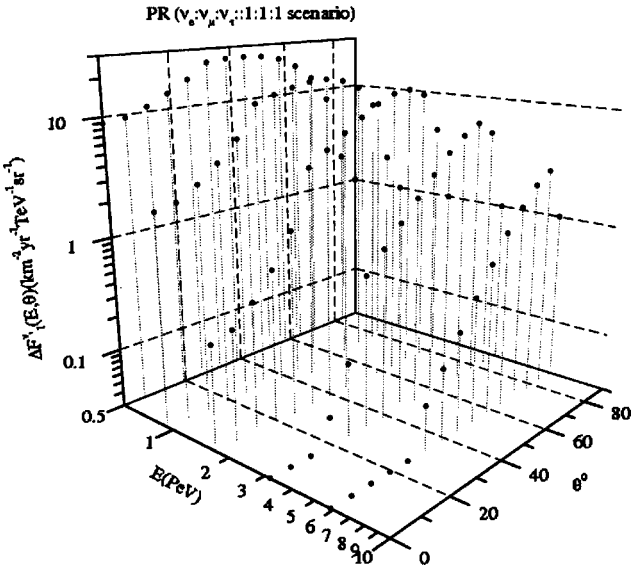

FIG. 14. Upward ν_τ flux difference $\Delta F_1^{\nu_\tau}(E,\theta)$ ($\mathrm{km}^{-2}\mathrm{yr}^{-1}\mathrm{TeV}^{-1}\mathrm{sr}^{-1}$) vs energy E (PeV) and nadir angle θ (deg), for Protheroe input flux model in the scenario $\nu_e:\nu_\mu:\nu_\tau::1:1:1$.

chosen to be the Protheroe model [11]; also the qualitative features of these plots, like the earlier plots, are model independent so it is not important to show the figures for all the models. We see in Fig. 9: (a) Even at energies $E=0.5$ PeV, the LSG1 and SM flux models are distinguishable; (b) in the ν_e, ν_μ, ν_τ::1, 1, 1 scenario, $\Delta F_1(E)$ and $\Delta F_2(E)$ are larger at lower energies, however, in contrast in the ν_e, ν_μ, ν_τ::1, 2, 0 scenario, they decrease with decreasing energy. This contrasting behavior of the two scenarios begins around 1 PeV for LSG1 and around 5 PeV for LSG2. This is expected because the stronger feed down effect due to taus causes $F_{SM}(E)$ in the ν_e, ν_μ, ν_τ::1, 1, 1 scenario to increase faster with decreasing energy than in the other scenario; however, $F_{LSG1}(E)$ and $F_{LSG2}(E)$ are not as different in the two scenarios because they are not as sensitive to tau regeneration. Hence, the overall result is decreasing flux difference for the ν_e, ν_μ, ν_τ::1, 2, 0 scenario and increasing flux difference for the other scenario. This happens at a lower energy in the LSG1 model due to the lower energy scale for LSG1 (Figs. 1, 2); (c) another important observation is that $\Delta F_1(E)$ is almost equal to $F_{SM}(E)$ after 3 PeV, which means if we want to differentiate the two models on the basis of the nadir angle integrated event rates, the best region in energy may be around 3 PeV, if the detector has large enough efficiency to detect this flux. However, obtaining larger fluxes for better statistics requires looking at lower energies. Though the model fluxes around energies as low as 100 TeV are larger, the percent difference between SM and LSG fluxes becomes smaller and smaller at energies below 0.5 PeV where SM cross sections are dominant; the total upward flux rises much faster than the flux difference, making it hard to differentiate between the two models. The atmospheric background is also larger at these energies, hence we did not find it interesting to show the fluxes below 0.5 PeV.

In Fig. 10 we plot the nadir angle integrated flux of ν_τ only. If we compare Figs. 9 and 10, we come up with the similar answer as we did for the flux integrated over energy $[\Delta F_1^{\nu_\tau}(E)]$: the upward ν_τ flux difference, $\Delta F_1^{\nu_\tau}(\theta)$, around 0.5 PeV is almost 3/4 of the total upward flux difference $\Delta F_1(\theta)$. This again gives one hope that the signals of low scale gravity may appear even around 0.5 PeV.

(iii) Plots of flux as a function of both energy and nadir angle. Figures 11–14 give the complete detail of the fluxes in the (E,θ) space for our flux example of Protheroe [11]. In Figs. 11 and 12 we plot the total upward flux in SM, $F_{SM}(E,\theta)$, and the total upward flux difference $\Delta F_1(E,\theta)$, respectively; Figs. 13 and 14 have similar plots for the ν_τ. We can see in these plots: (a) The difference is the largest around 80°, however, it is still increasing even at 0.5 PeV. Again, this may be surprising at first glance because below 1 PeV there is no significant contribution to the cross sections from LSG. However, the reason is simply that the cross section at a given energy will affect the neutrino flux at equal *and lower* energies due to feed down. Keeping this in mind, we can argue that the flux around 1 PeV or below gets more feed down from higher energies in SM because LSG black hole cross section, being the largest of all the cross sections, suppresses the feed down effect due to any process. (b) At higher energies the flux difference peaks at higher angles e.g. around 80°; the peak shifts to lower angles at lower energies. One may argue that the peak should always occur at the lowest nadir angle because the neutrinos will have more interactions as they pass through Earth with larger chord lengths, and hence the SM and LSG models' interaction will cause the flux differences to become larger and larger at lower angles and higher energies. However, this does not happen because the input fluxes at higher energies are so small that at lower nadir angles all the flux is either absorbed or fed down to lower energies; that is why we see the flux difference peak shifts towards 0° nadir angle at lower energies: feed down effect makes the difference, between SM and LSG, at higher energies appear at lower energies. (c) The ν_τ plots in Figs. 13 and 14 show us that the major contributor of the difference between SM and LSG is the ν_τ at lower energies. It contributes almost 3/4 of the total difference around 0.5 PeV and around 1/3 at 10 PeV. This feature is best seen in these full (E,θ)-space plots. Around energies 0.5 PeV, ν_τ plays an important role in probing new physics. At energies around 10 PeV and higher, ν_τ behaves more like ν_e and ν_μ; this is because around these energies the feed down due to taus, from even higher energies, is not a big effect both in SM and LSG. This is a result of larger tau decay lengths, smaller interaction lengths (see Figs. 1 and 2), and smaller fluxes at higher energies.

TABLE I. Flux ratios of the fluxes integrated over energy $E>0.5$ PeV at a fixed nadir angle $\theta=45°$, for SM, LSG with $M=2$ TeV ($G2$), and LSG with $M=1$ TeV ($G1$); $R1$, $R2$, and $R3$ are defined in Eqs. (16).

Model	$R1$			$R2$			$R3$		
	SM	*G*2	*G*1	*SM*	*G*2	*G*1	*SM*	*G*2	*G*1
WB	0.18	0.17	0.12	0.25	0.23	0.14	0.85	0.82	0.66
M(*B*)	0.15	0.12	0.06	0.29	0.20	0.07	1.61	1.26	0.73
PR	0.17	0.16	0.09	0.27	0.24	0.12	1.13	1.03	0.73
SDSS	0.18	0.18	0.12	0.24	0.24	0.15	0.83	0.82	0.66
1/*E*	0.10	0.05	0.02	0.22	0.09	0.02	2.84	1.60	0.80

Summarizing, we see that the above analysis discloses the flux structure in (E,θ) space: (i) Around 0.5 PeV, the flux difference peaks in the 40–60° region. The larger angles tend to wash out the difference between LSG and SM. (ii) Around 5 PeV, the difference peaks in the 75–80° region. (iii) At higher energies, one will have to look at even larger nadir angles to get any detectable up flux. In Tables I and II, we give different flux ratios $R1$, $R2$, and $R3$ defines as

$$R1=\frac{F^{\text{total}}(\text{up})}{F^{\text{total}}(\text{down})},\qquad R2=\frac{F_{\nu_\tau}(\text{up})}{F_{\nu_\tau}(\text{down})},$$

$$R3=\frac{F_{\nu_\tau}(\text{up})}{F_{\nu_e}(\text{up})+F_{\nu_\mu}(\text{up})}, \tag{16}$$

TABLE II. Flux ratios of the fluxes integrated over nadir angle θ at a fixed energy $E=5$ PeV, for SM, LSG with $M=2$ TeV (columns $G2$), and LSG with $M=1$ TeV (columns $G1$); $R1$, $R2$, and $R3$ are defined in Eqs. (16).

Model	$R1$			$R2$			$R3$		
	SM	*G*2	*G*1	*SM*	*G*2	*G*1	*SM*	*G*2	*G*1
WB	0.20	0.18	0.02	0.25	0.22	0.02	0.71	0.65	0.53
M(*B*)	0.28	0.22	0.02	0.45	0.30	0.02	1.12	0.84	0.56
PR	0.21	0.19	0.02	0.29	0.23	0.02	0.80	0.69	0.54
SDSS	0.19	0.18	0.02	0.23	0.20	0.02	0.66	0.62	0.53
1/*E*	0.43	0.24	0.02	0.82	0.35	0.02	1.72	0.93	0.57

in the ν_e, ν_μ, ν_τ::1, 1, 1 scenario, for SM, LSG with $M=2$ TeV (G2), and LSG with $M=1$ TeV (G1). These ratios reveal some interesting and useful features: (i) If we compare $R2$ and $R3$ with $R1$ in Tables I and II, we find that ν_τ flux indeed behaves differently in SM and LSG. (ii) In LSG, at higher energies, ν_e, ν_μ, and ν_τ tend to become identical as expected from larger decay length of taus at higher energies and larger black hole cross sections hence smaller feed down of ν_τ from tau decays; this effect is indeed seen for LSG (1 TeV) (see G1 in Table II); $R1$ and $R2$ tend to become equal and $R3$ tends to become 0.5 as expected (see G1 in Table II). The same will be true for LSG (2 TeV) at even higher energies. (iii) No matter which neutrino flux model is correct, even at energies as low as 0.5 PeV, we see a clear difference between SM and LSG (1 TeV) model (Table I); at higher energies, $E>10$ PeV, there should be a difference between LSG (2 TeV) and SM based on their comparison at 5 PeV (Table II). Our data at 10 PeV, which is not shown here, implies that, based on the flux ratios, the % difference between LSG (2 TeV) and SM at 10 PeV is bigger than the one between LSG (1 TeV) and SM at 5 PeV. (iv) Isolating ν_τ should help differentiate between SM and LSG, and may help to differentiate between different neutrino flux models given SM dynamics. For example, in Tables I and II, though $R1$ is similar for different flux models in the SM case, $R3$ shows some significant variation.

However, results of propagated WB and SDSS models are close to each other; they are similar because, though WB down flux at lower energies is much smaller than SDSS, WB flux falls like E^{-2} while SDSS goes like E^{-3} at higher energies giving a stronger feed down effect for the former, hence, their up-down flux ratios tend to be the same; the big difference between these models is that WB has much weaker flux at energies 0.1–10 PeV (Figs. 6 and 7). (v) The difference among flux models are largely washed out by the LSG dynamics at higher energies. For example, in Table II, $R1$ and $R2$ are the same for all the flux models given here when the LSG scale is 1 TeV. As mentioned above, to probe higher LSG scales, one must go to higher energy data which shows some sensitivity up to $M=5$ TeV [34].

V. EVENT RATES

Next we outline the formalism to calculate event rates for showers, muons, and taus. Our formalism adds some refinement to the event rate estimates [42,74]. In presenting event rates, we take our theoretical ''ICECUBE-like'' detector to be 1 km^3 of strings of optical modules deployed with 125 m horizontal spacing. Because rates of events depend on flux and cross section, the extra depletion of upward flux in the LSG models is somewhat compensated by the increased interaction probability of each neutrino that penetrates the detector effective volume.

(i) Shower rates. Neutrino-nucleon interactions at PeV energies and above initiate electromagnetic and hadronic showers which may produce a detectable radio or optical Cherenkov signal in detectors like RICE, AMANDA, ICECUBE. For shower rates in SM, we include both CC and NC interactions of ν_e and ν_τ but only NC interactions for ν_μ (CC interaction in this case gives muons which can be detected directly in detectors like AMANDA and ICECUBE). For LSG, we include both eikonal and black hole cross sections. For shower rates R_{shower} in LSG,

$$R_{shower} \cong A L^s_{eff} \rho N_A \sum_i \int_{E_0}^{\infty} dE^p_{\nu_i} F^i(E^p_{\nu_i}) \times \left(\sigma_{BH}(E^p_{\nu_i}) + \int_{E_{h0}/E^p_{\nu_i}}^{1} dy \frac{d\sigma^i_{CC+NC+EK}(E^p_{\nu_i}, y)}{dy} \right) \tag{17}$$

where A is the detector area and $L^s_{eff}=L_D+0.3$(km), as discussed below for shower rates, is the effective length of a detector of instrumental length L_D. $E^p_{\nu_i}$ is the primary neutrino energy, E_0 has to be greater than or equal to the minimum energy at which the flux is known, and E_{h0} is the minimum energy of the hadronic shower. The sum over ''i'' is to account for different neutrino flavors. With the exception of ν_e CC interaction, for which we must set $E_{h0}=0$ for the reason given below, we have to set $E_{h0}=E_0 \geqslant 1$ TeV as we do not know the flux below E_0 and hence cannot account for all the showers produced below E_0. One needs $E_{h0}>1$ TeV for the showers to be detectable. For the black hole we assume that it has equal probability of decaying into any SM particles, and that it will always give a shower of energy around E_0 and higher.

Two important points: (i) *We take the effective detector length L^s_{eff} as the instrumental detector length L_D plus 0.3 km. This is because, in addition to the showers produced inside the detector, a conservative estimate is that shower signal produced 0.15 km outside the detector, on any side, will easily reach the detector using a shower range of 0.3 km for optical modules*. This increases the shower rates by 30%. (ii) *For showers from ν_e CC interaction, there is no need to set a lower limit on y as the electron energy will add to the hadron energy to contribute to the shower signal (e.g. effectively one can set $E_{h0}=0$).* This increases the shower rates dramatically—30–50 %. This is because in this case we can set minimum $y=0$ and the CC cross section peaks around $y=0$ giving a large percentage of the total shower events.

(ii) Muon rates. ν_μ CC interaction and ν_τ CC interaction, with the tau decay $\tau \rightarrow \nu_\tau \nu_\mu \mu$, both are the sources of muons [84]. For the former case, muon rate R^{CC}_μ is given by

$$R_\mu^{CC} \cong A\rho N_A \int_{E_0}^{\infty} dE_{\nu_\mu}^p F^{\nu_\mu}(E_{\nu_\mu}^p) \times \int_0^{1-E_{\mu 0}/E_{\nu_\mu}^p} dy \frac{d\sigma_{CC}^{\nu_\mu}(E_{\nu_\mu}^p, y)}{dy} L_{eff}^{\mu}(E_{\nu_\mu}^p, y) \times \theta\left(\frac{R(E_\mu, E_{\mu 0})}{\rho} - (x_{\min}^{\mu track} + l^{show}) \right), \tag{18}$$

where $E_{\mu 0} = E_0$ for the same reason as given above for the shower rate. The $x_{\min}^{\mu track} \simeq 0.25$ km is the minimum muon track length required to detect a muon and $l^{show} \simeq 0.02$ km ($\ll x_{\min}^{\mu track}$) is the typical shower size (for PeV energies) of the shower produced at the ν_μ event vertex. The θ function guarantees the exclusion of muons whose range is too small for them to be detected. $L_{eff}^{\mu}(E_{\nu_\mu}^p, y)$ is the effective detector length for muon rates:

$$L_{eff}^{\mu}(E_{\nu_\mu}^p, y) = \frac{R(E_\mu(E_{\nu_\mu}^p, y), E_{\mu 0})}{\rho} + L_D - 2x_{\min}^{\mu track} - l^{show}, \tag{19}$$

where

$$\frac{R(E_\mu, E_{\mu 0})}{\rho} = \frac{1}{\rho\beta} \ln\left(\frac{\alpha + \beta E_\mu}{\alpha + \beta E_{\mu 0}} \right) \tag{20}$$

is the average electromagnetic range, in a matter of density ρ, of a muon of initial and final energies E_μ and $E_{\mu 0}$, respectively. Here $\alpha = 2.0$ MeV cm^2/g accounts for the muon energy loss due to ionization and $\beta = 4.2 \times 10^{-6}$ cm^2/g is due to pair production, bremsstrahlung, and photonuclear energy losses [75].

We should emphasize that *the effective detector length* $L_{eff}^{\mu}(E_{\nu_\mu}^p, y)$ *given above is the appropriate one for this case.* Our definition of the effective detector length works for any value of the muon range while $R(E_\mu, E_{\mu 0})/\rho$ works only for $R(E_\mu, E_{\mu 0})/\rho \gg L_D$.

Muon rate from the tau decay $\tau \to \nu_\tau \nu_\mu \mu$ is given by

$$R_\mu^{\tau \to \mu} \cong A\rho N_A \int_{E_0}^{\infty} dE_{\nu_\tau}^p F^{\nu_\tau}(E_\nu^p) \times \int_0^{1-E_{\tau 0}/E_{\nu_\tau}^p} dy \frac{d\sigma_{CC}^{\nu_\tau}(E_{\nu_\tau}^p, y)}{dy} \int_0^{\infty} dx \frac{e^{-x/\mathcal{L}_{dec}^{\tau}(E_\tau)}}{\mathcal{L}_{dec}^{\tau}(E_\tau)} \times \int_{E_{\mu 0}/E_\tau}^1 dz' \frac{dP^{\tau \to \mu}(z')}{dz'} L_{eff}^{\mu}(E_{\nu_\tau}^p, z') \times \theta\left(\left(\frac{R(z' E_\tau, E_{\mu 0})}{\rho} \right) - (x_{\min}^{\mu track} + l^{show}) \right), \tag{21}$$

where $\mathcal{L}_{dec}^{\tau}$ is defined in Eq. (13); $E_{\tau 0} = E_0$ for the same reason as given above for the shower and muon rate; $dP^{\tau \to \mu}(z')/dz'$ gives the relevant decay distribution with $E_\mu = z' E_\tau = z'(1-y) E_{\nu_\tau}^p$ [46], [2000]; $x_{\min}^{\mu track}$ and l^{show} are the same as defined above. L_{eff}^{μ} is defined in Eq. (19). The integration over x gives total probability that a tau will decay with a tau decay length between 0 and ∞. The θ function requires the muon range to be greater than the minimum distance required to detect a muon.

(iii) Tau rates. We discuss two types of events that are unique to the presence of taus and ν_τ [42,76–78]: (1) A tau produced in a ν_τ CC interaction *outside* the detector decays (excluding the decay $\tau \to \nu_\tau \mu \nu_\mu$) *inside* the detector a track and a shower:

$$R_\tau^{\tau dec}(1 \text{ shower}) \cong 0.83 A\rho N_A \int_{E_0}^{\infty} dE_{\nu_\tau}^p F^{\nu_\tau}(E_{\nu_\tau}^p) \times \int_0^{1-E_{\tau 0}/E_{\nu_\tau}^p} dy \frac{d\sigma_{CC}^{\nu_\tau}(E_{\nu_\tau}^p, y)}{dy} \times \left(\int_{x_{\min}^{\tau track} + 0.15(\text{km})}^{L_D + 0.3(\text{km})} dx L_{1eff}^{\tau}(x) \frac{e^{-x/\mathcal{L}_{dec}^{\tau}(E_\tau)}}{\mathcal{L}_{dec}^{\tau}(E_\tau)} + \left(L_{2eff}^{\tau} \int_{L_D + 0.3(\text{km})}^{\infty} dx \frac{e^{-x/\mathcal{L}_{dec}^{\tau}(E_\tau)}}{\mathcal{L}_{dec}^{\tau}(E_\tau)} \right) \right), \tag{22}$$

where

$$L_{1eff}^{\tau}(x) = (x - x_{\min - 0.15(\text{km})}^{\tau track}) \qquad L_{2eff}^{\tau} = (L_D + 0.15(\text{km}) - x_{\min}^{\tau track}), \tag{23}$$

where $E_{\tau 0} = E_0$ for the same reason as given above for the shower and muon rate. The 0.83 factor is to exclude the decay $\tau \to \nu_\tau \mu \nu_\mu$ which has a branching ratio of ~ 0.17, and $x_{\min}^{\tau track} \simeq 0.25(\text{km})$ is the minimum tau track length required to detect a tau. We have assumed that all the showers produced in these events will be detectable, so we do not need tau decay distribution function. This is a reasonable assumption as we will choose $E_0 = E_{\tau 0} = 0.5$ PeV which means almost all of the showers produced from tau decay will be above the detector threshold of ~ 0.001 PeV. The lower limit for x integration assures the tau decay length large enough for the tau to be separately detected from the shower. The expression given for these events in Ref. [42] includes some *shower-track-shower* events too. The expression above gives *only track-shower* events by using the x dependent effective length where x is smaller than $L_D + 0.3(\text{km})$. Moreover, we have included the 0.3(km) in the x integration limit and 0.15(km) in the expression for L_{2eff}^{τ}. These numbers follow from the reasoning given above in discussion of shower rates.

(2) A tau produced in a ν_τ CC interaction *inside* the detector decays (excluding the decay $\tau \to \nu_\tau \mu \nu_\mu$) *inside* the detector giving a shower, a track, and another shower. These are so-called double bang events [76]:

TABLE III. Up and down events (yr^{-1}) for $E \geqslant 0.5$ PeV in the scenario 1:1:1; all upward events are integrated over nadir angle $\theta \leqslant 84°$; down showers are integrated over angle but muons and taus are not (see text for details).

	showers $\left(\frac{\text{up}}{\text{down}}\right)$			muons $\left(\frac{\text{up}}{\text{down}}\right)$			taus $\left(\frac{\text{up}}{\text{down}}\right)$		
	SM	*G*2	*G*1	*SM*	*G*2	*G*1	*SM*	*G*2	*G*1
WB	$\frac{2.6}{11}$	$\frac{2.7}{24}$	$\frac{3.1}{201}$	$\frac{3.0}{3.3}$	$\frac{2.7}{3.3}$	$\frac{1.1}{3.3}$	$\frac{0.11}{0.13}$	$\frac{.074}{0.13}$	$\frac{0.0086}{0.13}$
SD	$\frac{163}{622}$	$\frac{167}{748}$	$\frac{202}{4725}$	$\frac{176}{142}$	$\frac{165}{142}$	$\frac{74}{142}$	$\frac{4.7}{4.6}$	$\frac{4.0}{4.6}$	$\frac{0.54}{4.6}$
MB	$\frac{3.0}{30}$	$\frac{3.1}{195}$	$\frac{2.2}{1898}$	$\frac{6.4}{18}$	$\frac{3.6}{18}$	$\frac{0.66}{18}$	$\frac{0.46}{0.86}$	$\frac{0.20}{0.86}$	$\frac{0.01}{0.86}$
PR	$\frac{32}{182}$	$\frac{33}{534}$	$\frac{34}{5284}$	$\frac{50}{73}$	$\frac{38}{73}$	$\frac{12}{73}$	$\frac{2.4}{3.5}$	$\frac{1.5}{3.5}$	$\frac{0.13}{3.5}$

$$R_\tau^{\tau dec}(2\ \text{shower}) \cong 0.83 A \rho N_A \int_{E_0}^{\infty} dE_{\nu_\tau}^p F^{\nu_\tau}(E_{\nu_\tau}^p) \times \int_0^{1-E_{\tau 0}/E_{\nu_\tau}^p} dy \frac{d\sigma_{CC}^{\nu_\tau}(E_{\nu_\tau}^p, y)}{dy} \times \int_{x_{\min}^{\tau track}+l^{show}}^{L_D+0.3(\text{km})} dx \frac{e^{-x/\mathcal{L}_{dec}^{\tau}(E_\tau)}}{\mathcal{L}_{dec}^{\tau}(E_\tau)} L_{3eff}^{\tau}(x), \tag{24}$$

where

$$L_{3eff}^{\tau}(x) = (L_D + 0.3(\text{km}) - x) \tag{25}$$

and all the other symbols have been defined above.

In addition to the above events for tagging taus, we have looked at the possibility of detecting taus from the decay $\tau \rightarrow \nu_\tau \mu \nu_\mu$ provided the tau decays *inside* the detector. These events have smaller rate than double bang or single shower events. Details of this calculation will be given elsewhere.

TABLE IV. Ratios of the ratios; here $RR1$=showers down/muons up and $RR2$=taus down/taus up.

	$\frac{RR1_{G2}}{RR1_{SM}}$		$\frac{RR1_{G1}}{RR1_{SM}}$		$\frac{RR2_{G2}}{RR2_{SM}}$	$\frac{RR2_{G1}}{RR2_{SM}}$
	1:2:0	1:1:1	1:2:0	1:1:1		
WB	$\frac{4.5}{1.7}=2.7$	$\frac{8.8}{3.6}=2.4$	$\frac{93}{1.7}=56$	$\frac{183}{3.6}=50$	1.5	13
SD	$\frac{2.1}{1.6}=1.3$	$\frac{4.5}{3.5}=1.3$	$\frac{34}{1.6}=21$	$\frac{64}{3.5}=18$	1.2	8.7
MB	$\frac{30}{2.1}=14$	$\frac{54}{4.7}=11$	$\frac{1571}{2.1}=735$	$\frac{2875}{4.7}=610$	2.3	46
PR	$\frac{7.4}{1.6}=4.7$	$\frac{14}{3.6}=3.9$	$\frac{249}{1.6}=157$	$\frac{440}{3.6}=121$	1.6	18

TABLE V. Same as Table III but with energy threshold 5 PeV.

	showers $\left(\frac{\text{up}}{\text{down}}\right)$			muons $\left(\frac{\text{up}}{\text{down}}\right)$			taus $\left(\frac{\text{up}}{\text{down}}\right)$		
	SM	*G*2	*G*1	*SM*	*G*2	*G*1	*SM*	*G*2	*G*1
WB	$\frac{0.26}{2.9}$	$\frac{0.33}{13}$	$\frac{0.15}{151}$	$\frac{0.3}{0.84}$	$\frac{0.14}{0.84}$	$\frac{.002}{0.84}$	$\frac{0.07}{0.11}$	$\frac{0.04}{0.11}$	$\frac{.001}{0.11}$
SD	$\frac{11}{94}$	$\frac{15}{188}$	$\frac{8.7}{2714}$	$\frac{8.4}{14}$	$\frac{5.6}{14}$	$\frac{0.1}{14}$	$\frac{2.5}{3.1}$	$\frac{1.8}{3.1}$	$\frac{0.05}{3.1}$
MB	$\frac{1.2}{21}$	$\frac{1.4}{157}$	$\frac{0.41}{1602}$	$\frac{2.0}{9.2}$	$\frac{0.66}{9.2}$	$\frac{.006}{9.2}$	$\frac{0.41}{0.83}$	$\frac{0.16}{0.83}$	$\frac{.003}{0.83}$
PR	$\frac{6.5}{82}$	$\frac{8}{371}$	$\frac{2.9}{4178}$	$\frac{8.5}{26}$	$\frac{3.7}{26}$	$\frac{.04}{26}$	$\frac{1.9}{3.0}$	$\frac{0.93}{3.0}$	$\frac{0.02}{3.0}$

VI. RESULTS AND DISCUSSION FOR EVENT RATES

The results for event rates are summarized in Tables III–VI. The event rates at angles below 60° turn out to be very small for current detectors, hence, we show events integrated to $\theta = 84°$ nadir angle.

In Table III we give different upward and down events per year, in the scenario 1:1:1, for a 1 km^3 detector in ice. Our down shower events have been integrated over angle, however, the down tau and down muon events correspond to near horizon events. The showers contain events due to all neutrino flavors. These shower events in 1:1:1 scenario are 30–40% larger than 1:2:0 scenario (not shown here). This is because, in the latter, we are excluding ν_μ CC interaction and also the total flux is smaller due to the absence of tau regeneration effect. Upward muons (muon up) contain muons from ν_μ CC interaction and the muonic tau decay. The muons in 1:1:1 scenario are about 40% smaller than 1:2:0 scenario (not shown). They are not exactly 50% of the latter due to the contribution from tau decays. The upward taus (taus up) contain all three types of events described above [e.g. tau up=(*track*−*shower*)+(*shower*−*track*−*shower*)+$\tau \rightarrow \nu_\tau \mu \nu_\mu$]. The ratio (*track*−*shower*)/(*shower*−*track*−*shower*), not shown here, is very sensitive to the flux model and can be anywhere between 0.7 to 1.7. The τ

TABLE VI. Same as Table IV but with energy threshold 5 PeV.

	$\frac{RR1_{G2}}{RR1_{SM}}$		$\frac{RR1_{G1}}{RR1_{SM}}$		$\frac{RR2_{G2}}{RR2_{SM}}$	$\frac{RR2_{G1}}{RR2_{SM}}$
	1:2:0	1:1:1	1:2:0	1:1:1		
WB	11	9.3	8400	7826	1.7	74
SD	3.2	3.0	2481	1419	1.4	48
MB	27	23	3.0*e*4	2.7*e*4	2.6	161
PR	12	10	1.2*e*4	1.0*e*4	2.0	100

$\rightarrow \nu_\tau \mu \nu_\mu$ tau events are always the smallest—less than 50% of the smaller of the single shower and double bang. While muons show differences between LSG (1 TeV) and SM, the up-to-down showers and tau event ratios show a clearer differentiation between the two (Table III). The number of events, though marginal for ν_τ's in WB and MB, are sufficient to make a clear distinction from SM for LSG (1 TeV) and distinction in some cases for LSG (2 TeV) in several years of data taking. The up tau events in the LSG (1 TeV) are especially severely suppressed as compared to the SM. This again reflects the fact that tau decay is playing a much weaker role in LSG (1 TeV) (see Sec. IV). However, as expected, taus play a similar role in SM and LSG (2 TeV), though some suppression of ν_τ is evident for LSG (2 TeV) in Tables III and IV. In Table IV, we see the LSG/SM ratio of the ratios, as defined in the table caption, strongly differentiates SM from LSG (1 TeV) in both of the flavor scenarios. *In fact, these ratios have very weak dependence on the flavor scenario.* They are spectacularly large in every flux model. Even LSG (2 TeV) is clearly distinguished in all but the SDSS model. In the latter, the number of events is large enough that one may hope to discriminate between LSG (2 TeV) and SM.

We show similar tables with an energy threshold at 5 PeV (Tables V and VI). Here we see the tau events did not change much in SM and LSG (2 TeV) model. However, in LSG (1 TeV) up tau events have decreased by an order of magnitude, generally with enough down events to make them even more useful in differentiating between the two at 5 PeV as compared to 0.5 PeV. Although not shown here, by comparing 5 PeV and 0.5 PeV results for showers and muons one expects that LSG (2 TeV) model around 10 PeV thresholds will differ from SM to the extent that LSG (1 TeV) does from SM around 0.5 PeV. However, the event rates may be too small to do a statistical analysis.

Looking at the event rates for different flux models in Table III, we see the PR and SDSS flux models provide large enough events to do a statistical analysis. For WB and MB models, only the down shower rates in LSG (1 TeV) are large enough to differentiate it from the SM by looking at the up-to-down shower ratios.

VII. SUMMARY OF RESULTS AND CONCLUSION

We found complete numerical solutions to the system of coupled equations that include the most important effects for transport through Earth of ν_e, ν_μ, ν_τ and τ fluxes above 0.5 PeV. In Fig. 4, we presented results of angular distributions of total neutrino flux in our example of the diffuse flux model by Protheroe [11], however, the qualitative features of this figure are common to the other flux models [Mannheim (B) [12], Waxman Bahcall [10], and SDSS [9]]. Fluxes in this figure are integrated from 0.5 PeV upward, showing the effects of including low scale gravity enhancement to the lepton deep inelastic cross sections, *with no ν_τ and full ν_τ mixing into the incident flux.* This figure also show that the ν_τ regeneration from τ decay enhances the ''through Earth,'' or ''upward'' fluxes significantly more in the standard model than in the models with low scale gravity enhancements included, as seen on the curves where ν_τ is mixed into the flux incident on Earth. The standard model flux is obviously higher at nadir angles smaller than 80°, while the differences between the fluxes with standard model interactions only and those with low scale gravity included are much larger at small nadir angles in the case that ν_τ is mixed into the incident flux than in the case when it is not. Next in Figs. 5–8, we showed the equivalent angular distributions for the ν_τ flux alone to emphasize the observation just summarized; that is, as compared to ν_e and ν_μ, ν_τ can serve better to differentiate between SM and LSG at energies below 10 PeV.

As established by the angular distribution graphs, the qualitative features are shared by all the models, so we gave only the Protheroe model results in plotting the energy distribution of flux integrated over angles in the range from 0.5 PeV to 20 PeV in Figs. 9 and 10. These plots show that in this energy range, the low scale gravity interactions rapidly suppress the upward flux compared to the standard model. They also indicate the fact that the regeneration of ν_τ flux is much less significant when low scale gravity is turned on, as clearly indicated by the flux difference curves in the energy range between 0.5 PeV and 2.0 PeV.

In the series of graphs from Figs. 11 through 14, we displayed the three-dimensional plots of the total and *ν_τ-only* fluxes for the standard model and for the low scale gravity, $M=1$ TeV case. These indicate in detail where the maximum flux differences are in angle and energy.

Next we looked at the flux ratios $R1$, $R2$, and $R3$ as defined in Eqs. (16). The results are given in Tables I and II. Here again the distinction between ν_τ and $\nu_\mu + \nu_e$ fluxes is evident. The distinctions among flux models are largely washed out by the LSG dynamics at higher energies. For example, in Table II, $R1$ and $R2$ are the same for all the flux models given here.

In Secs. V and VI we presented the defining equations for our shower, muon and tau rates and the results of our rate calculation. The story is summarized in Tables III–VI. Using a cutoff of 0.5 PeV, we found that the events rates in showers and muon categories are large enough to make meaningful statements about the distinction between SM and LSG with 1 TeV, in all flux models and both flavor scenarios with 2–3 years of running. An interesting feature of the LSG (2 TeV) entries in Tables III and IV is that the down shower events may be enhanced enough compared to SM to distinguish between the two in WB, MB, and PR, and possibly SD too. The ratio of ratios in Tables IV and VI compares the LSG shower down–muon up ratios to the ones for SM. Table IV and VI also show the same for taus down–taus up. This diagnostic is especially sensitive to the difference between SM and LSG. It also shows us that this ratio of the ratios for showers and muons is almost the same in both of the flavor scenarios. The importance of the taus in differentiating between SM and LSG (1 TeV) is realized by looking at the tagged tau events (Tables IV and VI). For tagged tau events, the difference between LSG (1 TeV) and the SM varies from an order of magnitude to two orders of magnitude for energy thresholds of 0.5–5 PeV. However, we caution the reader again that the statistics are low in this case. *Basically the tau story can be summarized by saying that any upward tau*

event establishes (1) ν_τ's presence in the neutrino flux incident on Earth and (2) exclusion of LSG with 1 TeV scale or any model of enhanced cross section of comparable size in the 1–10 PeV range.

The 5 PeV threshold results in Tables V and VI show the same patterns as in the 0.5 PeV tables. The distinction between SM and LSG (2 TeV) are now sharper in the ratios, but the statistics in some cases are low, so that one needs to have 5–10 years of data to draw strong conclusions that apply to all flux models.

We conclude on the basis of our flux and event rate study that with a threshold of 0.5 PeV, the shower and muon event ratios have sufficient events in all flux and lepton flavor models to make clear distinctions between SM and LSG with a mass scale 2 TeV and below. Going above 2 TeV, one finds that whether distinctions can be made depends upon the flux model. The situation is not so clear. Because the requirements on ν_τ identification are so stringent, only a few events to a fraction of an event will be expected, depending upon flux model, up or down event and LSG scale value. One point is perfectly clear: any upward tau event excludes LSG with a scale around 1 TeV.

Given the intense experimental activity in the field [79–82], we expect that data will yield many insights in the coming decade when analyzed with techniques like the ones presented here.

ACKNOWLEDGMENTS

We thank Pankaj Jain for many helpful comments and for use of his propagation programs at the early stage of this work. Shahid Hussain thanks M. H. Reno, J. Pumplin, and C. Hettlage for email exchange and discussions. This work was supported in part by The Department of Energy under Grant No. DE-FG03-98ER41079. We used the computational facilities of the Kansas Center for Advanced Scientific Computing for part of this work.

[1] KamiokandeII Collaboration, K. Hirata *et al.*, Phys. Rev. Lett. **58**, 1490 (1987).
[2] IMB Collaboration, R. Bionta *et al.*, Phys. Rev. Lett. **58**, 1494 (1987).
[3] For a recent review, see P. Biermann and G. Sigl, in *Introduction to Cosmic Rays*, edited by M. Lemoine and G. Sigl, Lecture Notes in Physics, Vol. 576 (2001), p. 1.
[4] K. Greisen, Phys. Rev. Lett. **16**, 748 (1966); G. Zatsepin and V. Kuzmin, Pis'ma Zh. Éksp. Teor. Fiz. **4**, 114 (1966) [JETP Lett. **4**, 78 (1966)].
[5] Examples of GZK generated neutrino fluxes are R. Engel, D. Seckel, and I. Stanev, Phys. Rev. D **64**, 093010 (2001); O.E. Kalashev, V.A. Kuzmin, D.V. Semikoz, and G. Sigl, *ibid.* **66**, 063004 (2002); Z. Fodor, S.D. Katz, A. Ringwald, and H. Tu, J. Cosmol. Astropart. Phys. **11**, 015 (2003). The GZK fluxes are negligible in the 0.5–50 PeV region that determines the event rates calculated in this paper.
[6] D. Bird *et al.*, Astrophys. J. **441**, 144 (1995).
[7] For the latest AGASA Collaboration UHE cosmic ray spectrum results, see http://www-akeno.icrr.u-tokyo.ac.jp/AGASA.
[8] The High Resolution Fly's Eye Collaboration, T. Abu-Zayyad *et al.*, astro-ph/0208243.
[9] F.W. Stecker, C. Done, M. Salamon, and P. Sommers, Phys. Rev. Lett. **66**, 2697 (1991); **69**, 2738(E) (1992).
[10] J. Bahcall and E. Waxman, Phys. Rev. D **64**, 023002 (2001).
[11] R.J. Protheroe, astro-ph/9607165.
[12] K. Mannheim, Astropart. Phys. **3**, 295 (1995).
[13] A.P. Szabo and R.J. Protheroe, Astropart. Phys. **2**, 375 (1994).
[14] R. Engel, D. Seckel, and T. Stanev, Phys. Rev. D **64**, 093010 (2001).
[15] G. Sigl, S. Lee, D.N. Schramm, and P. Coppi, Phys. Lett. B **392**, 129 (1997).
[16] U.F. Wichoski, J.H. Macgibbon, and R.H. Brandenberger, Phys. Rev. D **65**, 063005 (2002).
[17] N. Arkani-Hamed, S. Dimopoulos, and G. Dvali, Phys. Lett. B **429**, 263 (1998).
[18] L. Randall and R. Sundrum, Phys. Rev. Lett. **83**, 3370 (1999).
[19] I. Antoniadis, N. Arkani-Hamed, S. Dimopoulos, and G. Dvali, Phys. Lett. B **436**, 257 (1998).
[20] The AMANDA Collaboration, J. Ahrens *et al.*, Phys. Rev. Lett. **90**, 251101 (2003).
[21] W. Rhode *et al.*, Astropart. Phys. **4**, 217 (1996).
[22] MACRO Collaboration, M. Ambrosio *et al.*, Astropart. Phys. **19**, 1 (2003).
[23] Zh.-A. Dzhilkibaev *et al.*, Proc. Int. Conf. on Neutrino Telescopes, Venice, 2001; astro-ph/0105269.
[24] S. Yoshida *et al.*, Proc. 27th ICRC **3**, 1146 (2001).
[25] AMANDA Collaboration, S. Hundertmark, Proceedings of the 28th ICRC, Tsukuba, Japan, 2003, p. 1309.
[26] R. Balusaitas *et al.*, Phys. Rev. D **31**, 2192 (1995).
[27] RICE Collaboration, S. Seunarine, Proceedings of the 28th ICRC, Tsukuba, Japan, 2003, p. 1337.
[28] P. Gorham, K. Liewer, C. Naudet, D. Saltzberg, and D. Williams, astro-ph/0102435.
[29] Auger Collaboration, J. Bleumer, Proceedings of the 28th ICRC, Tsukuba, Japan, 2003.
[30] ICECUBE Collaboration, S. Yoshida, in Proceedings of the International Workshop on UHE Neutrino Telescopes, Chiba, Japan, 2003.
[31] For more on detectors, visit the website: http://www.hep.net/experiments/all_sites.html.
[32] G. Frichter, D. McKay, and J. Ralston, Phys. Rev. Lett. **74**, 1508 (1995); R. Gandhi, C. Quigg, M. Reno, and I. Sarcevic, Astropart. Phys. **5**, 81 (1996); Phys. Rev. D **58**, 093009 (1998).
[33] G. Domokos and S. Kovesi-Domokos, Phys. Rev. Lett. **82**, 1366 (1999); S. Nussinov and R. Shrock, Phys. Rev. D **59**, 105002 (1999); P. Jain, D. McKay, S. Panda, and J. Ralston, Phys. Lett. B **484**, 267 (2000).
[34] P. Jain, D. McKay, S. Panda, and J. Ralston, Phys. Rev. D **66**, 065018 (2002).
[35] S. Nussinov and R. Shrock, Phys. Rev. D **64**, 047702 (2001); A. Jain, P. Jain, D. McKay, and J. Ralston, hep-ph/0011310; A. Jain, P. Jain, D. McKay, and J. Ralston, Int. J. Mod. Phys. A

17, 533 (2002); C. Tyler, A. Olinto, and G. Sigl, Phys. Rev. D **63**, 055001 (2001); L. Anchordoqui, H. Goldberg, T. McCauley, T. Paul, S. Reucroft, and J. Swain, *ibid.* **63**, 124009 (2001); M. Kachelriess and M. Plumacher, *ibid.* **62**, 103006 (2000).
[36] J. Feng and A. Shapere, Phys. Rev. Lett. **88**, 021303 (2002); A. Anchordoqui and H. Goldberg, Phys. Rev. D **65**, 047502 (2002).
[37] A. Ringwald and H. Tu, Phys. Lett. B **525**, 135 (2002).
[38] M. Kowalski, A. Ringwald, and H. Tu, Phys. Lett. B **529**, 1 (2002).
[39] L. Anchordoqui, J. Feng, H. Goldberg, and A. Shapere, Phys. Rev. D **66**, 103002 (2002).
[40] S.I. Dutta, M.H. Reno, and Ina Sarcevic, Int. J. Mod. Phys. A **18**, 4085 (2003).
[41] J. Jones, I.M. Mocioiu, M.H. Reno, and I. Sarcevic, Phys. Rev. D (to be published), hep-ph/0308042.
[42] J.F. Beacom, N.F. Bell, D. Hooper, S. Pakvasa, and T.J. Weiler, Phys. Rev. D **68**, 093005 (2003).
[43] F. Halzen and D. Saltzberg, Phys. Rev. Lett. **81**, 4305 (1998).
[44] V.A. Naumov and L. Perrone, Astropart. Phys. **10**, 239 (1999).
[45] J. Beacom, P. Crotty, and E. Kolb, Phys. Rev. D **66**, 021302(R) (2002).
[46] S.I. Dutta, M.H. Reno, and I. Sarcevic, Phys. Rev. D **62**, 123001 (2000); **66**, 077302 (2002).
[47] F. Becattini and S. Bottai, Astropart. Phys. **15**, 323 (2001); S. Bottai and S. Giurgola, *ibid.* **18**, 539 (2003).
[48] C. Hettlage and K. Mannheim, Nucl. Phys. B (Proc. Suppl.) **95**, 165 (2001).
[49] D. Fargion, Astrophys. J. **570**, 909 (2002).
[50] J.L. Feng, Peter Fisher, Frank Wilczec, and Terri M. Yu, Phys. Rev. Lett. **88**, 161102 (2002).
[51] A. Kusenko and T.J. Weiler, Phys. Rev. Lett. **88**, 161101 (2002).
[52] J. Alvarez-Muñiz, F. Halzen, T. Han, and D. Hooper, Phys. Rev. Lett. **88**, 021301 (2002); J. Alvarez-Muñiz, J. Feng, F. Halzen, T. Han, and D. Hooper, Phys. Rev. D **65**, 124015 (2002).
[53] W. H. Press, B. P. Flannery, S. A. Teukolsky, and William T. Vetterling, *Numerical Recipes in Fortran: the Art of Scientific Computing*, 2nd ed. (Cambridge University Press, Cambridge, England, 1992).
[54] J. Pumplin, D.R. Stump, J. Huston, H.L. Lai, P. Nadolsky, and W.K. Tung, J. High Energy Phys. **07**, 012 (2002).
[55] D. Fargion, astro-ph/9704205.
[56] R. Gandhi, C. Quigg, M.H. Reno, and I. Sarcevic, Phys. Rev. D **58**, 093009 (1998).
[57] P. Jain, D. McKay, S. Panda, and J. Ralston, Phys. Lett. B **484**, 267 (2000).
[58] H.L. Lai *et al.*, Phys. Rev. D **55**, 1280 (1997).
[59] S. Dimopoulous and G. Landsberg, Phys. Rev. Lett. **87**, 161602 (2001); S. Giddings and S. Thomas, Phys. Rev. D **65**, 056010 (2002).
[60] R.C. Myers and M.J. Perry, Ann. Phys. (N.Y.) **172**, 304 (1986).
[61] L. Anchordoqui, J. Feng, H. Goldberg, and A. Shapere, Phys. Rev. D **65**, 124027 (2002).
[62] E.J. Ahn, M. Ave, M. Cavaglia, and A.V. Olinto, Phys. Rev. D **68**, 043004 (2003).
[63] H. Yoshino and Y. Nambu, Phys. Rev. D **68**, 024009 (2003).
[64] D. Ida, K.-y. Oda, and S.C. Park, Phys. Rev. D **67**, 064025 (2003).
[65] R. Emparan, Phys. Rev. D **64**, 024025 (2001).
[66] R. Emparan, M. Masip, and R. Rattazzi, Phys. Rev. D **65**, 064023 (2002).
[67] G. Giudice, R. Rattazzi, and J. Wells, Nucl. Phys. **B630**, 293 (2002).
[68] A. Dziewonski, in *The Encyclopedia of Solid Earth Geophysics*, edited by David E. Jones (Van Nostrand Reinhold, New York, 1989), p. 331.
[69] Particle Date Group, K. Hagiwara *et al.*, Phys. Rev. D **66**, 010001 (2002).
[70] T. K. Gaisser, *Cosmic Rays and Particle Physics* (Cambridge University Press, Cambridge, England, 1990).
[71] P. Lipari, Astropart. Phys. **1**, 195 (1993).
[72] H. Athar, King-man Cheung, Guey-Lin Lin, and Jie-Jun Tseng, Astropart. Phys. **18**, 581 (2003); L. Pasquali and M.H. Reno, Phys. Rev. D **59**, 093003 (1999).
[73] The ICECUBE Project, http://www.ssec.wisc.edu/a3ri/icecube.
[74] S.I. Dutta, M.H. Reno, and I. Sarcevic, Phys. Rev. D **62**, 123001 (2000).
[75] S.I. Dutta, M.H. Reno, and I. Sarcevic, Phys. Rev. D **63**, 094020 (2001).
[76] J.G. Learned and S. Pakvasa, Astropart. Phys. **3**, 267 (1995).
[77] J. Alvarez-Muniz and F. Halzen, ''Detection of Tau Neutrinos in IceCube,'' 1999, http://icecube.wisc.edu/science/sci-tech-docs/
[78] H. Athar, G. Parente, and E. Zas, Phys. Rev. D **62**, 093010 (2000).
[79] AMANDA Collaboration, F. Halzen *et al.*, in *Proceedings of the 26th International Cosmic Ray Conference (ICRC 99)*, Salt Lake City, 1999, edited by B. L. Dingus, D. B. Kieda, and M. H. Salamon (AIP, New York, 2000), pp. 428–431; ANTARES Collaboration, T. Montaruli, Nucl. Phys. B (Proc. Suppl.) **110**, 513 (2002); Baikal Collaboration, V. Balkanov *et al.*, *ibid.* **110**, 504 (2002); NESTOR Collaboration, P. Greider, *ibid.* **97**, 105 (2000); RICE Collaboration, I. Kravchenko *et al.*, Astropart. Phys. **19**, 15 (2003); The ICECUBE Project, http://www.ssec.wisc.edu/a3ri/icecube
[80] AMANDA Collaboration, F. Halzen *et al.*, in Proceedings of the 26th International Cosmic Ray Conference (ICRC 99) (Ref. [79]), pp. 428-431.
[81] RICE Collaboration, I. Kravchenko *et al.*, Astropart. Phys. **19**, 15 (2003).
[82] RICE Collaboration, I. Kravchenko *et al.*, Astropart. Phys. **20**, 195 (2003).
[83] All of our fluxes include neutrinos and antineutrinos.
[84] We do not include here the taus from ν_τ CC interaction that will be mistaken by the detector as muons.